질소 순환 소재 합성 공정 최신전략
Synthetic Strategies of Nitrogen Cycle Reaction Catalysts and Materials

Uk Sim, Ph. D.

Nanomaterials for Energy & Environment Laboratory
www.uksim.org

N_2 Activation by plasma treatment

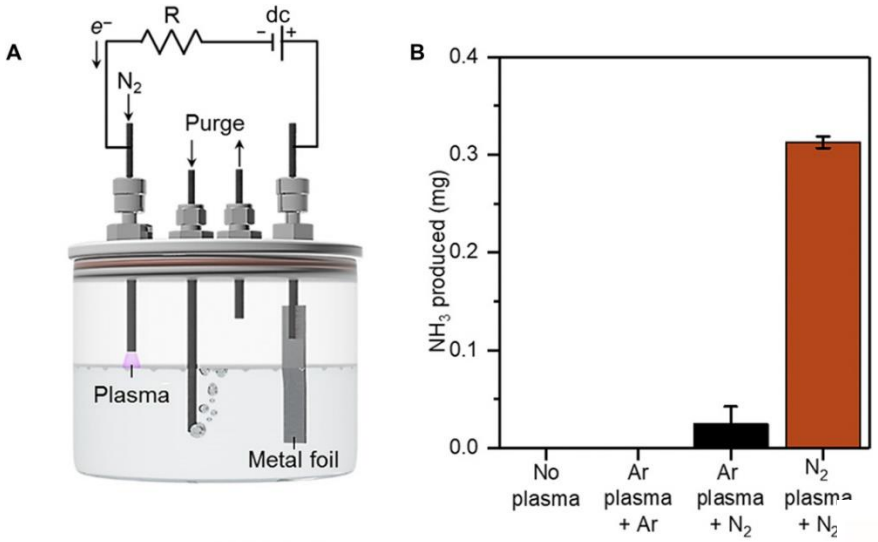

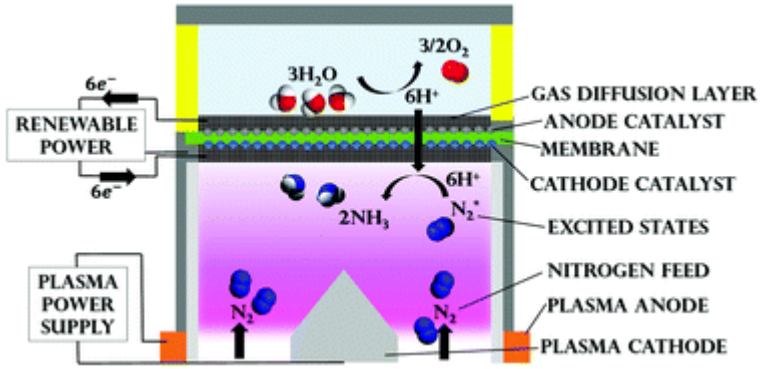

Chem. Commun., 2018,54, 13347-13350

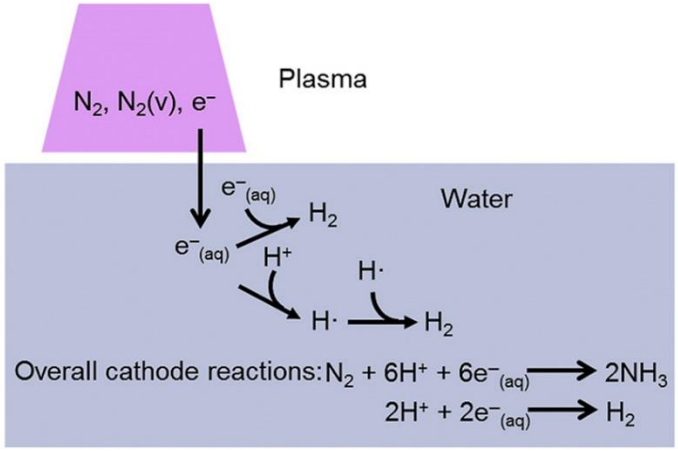

Science Advances 2019, 5 (1) 5778

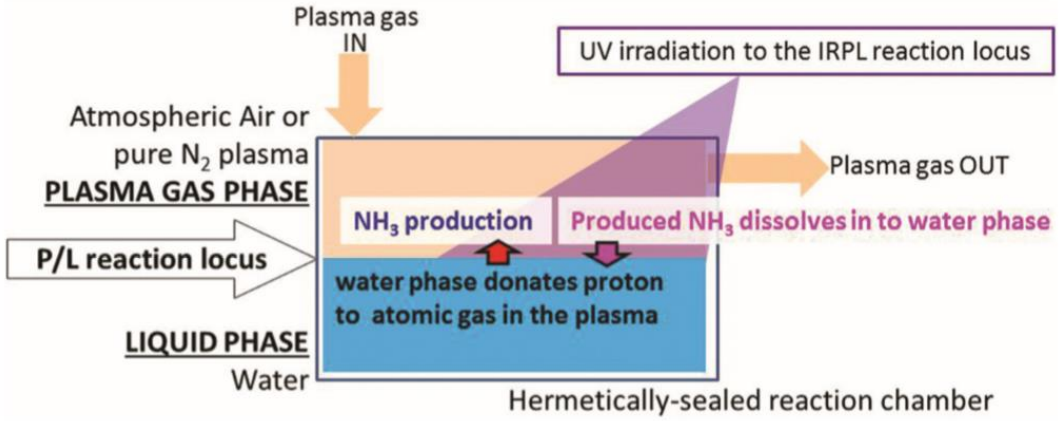

Green Chem., 2016,18, 4536–4541

Strategies for N_2 binding to the catalyst surface

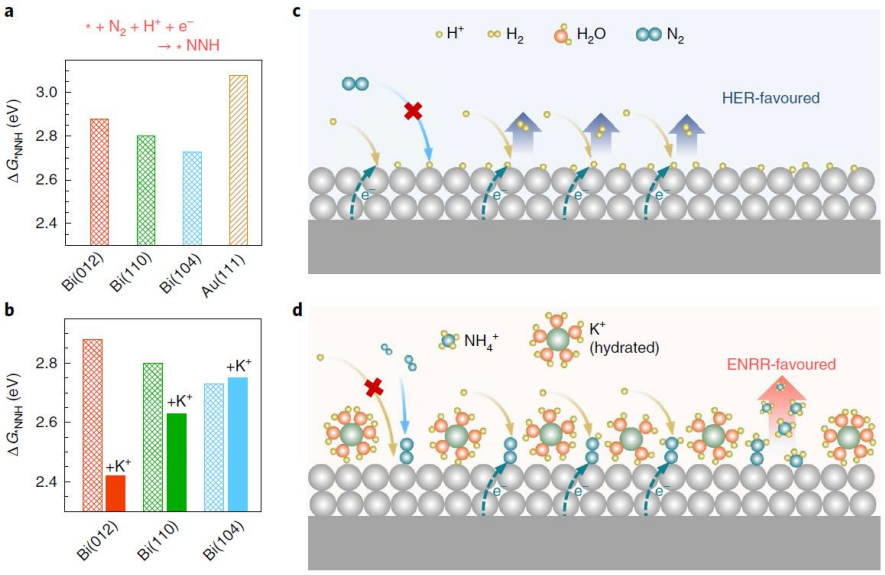

Nature Catalysis 2019
https://doi.org/10.1038/s41929-019-0241-7

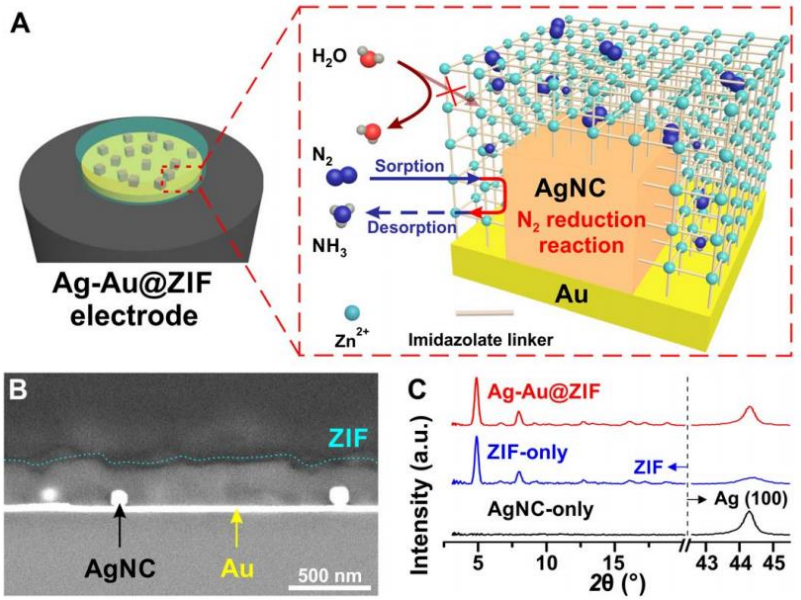

Science Advances 09 Mar 2018:
Vol. 4, no. 3, eaar3208

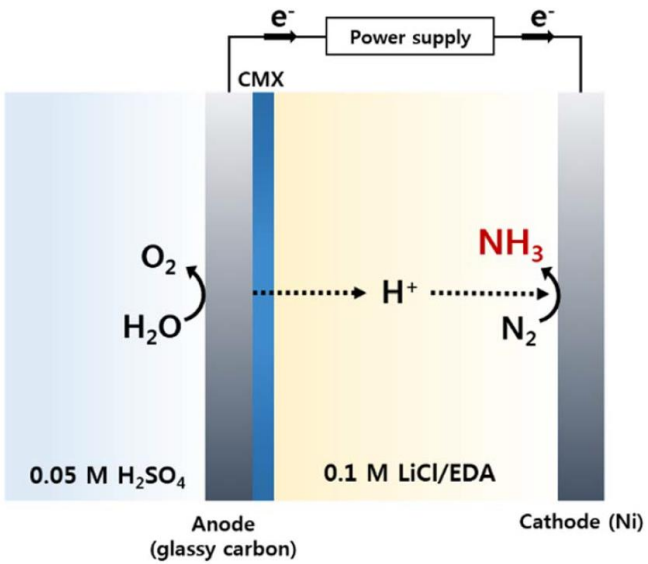

J. Electrochem. Soc. **2016**, 163 (14) F1523

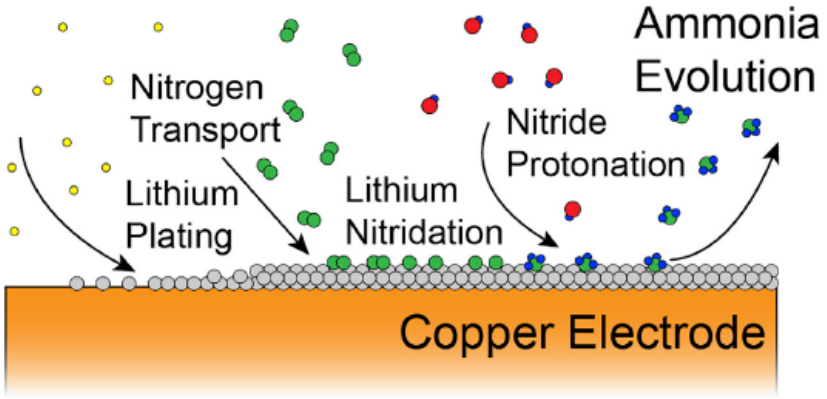

Joule Volume 3, Issue 4, 17 April 2019, Pages 1127-1139

Ammonia Production using Water and N_2 under RT and 1atm

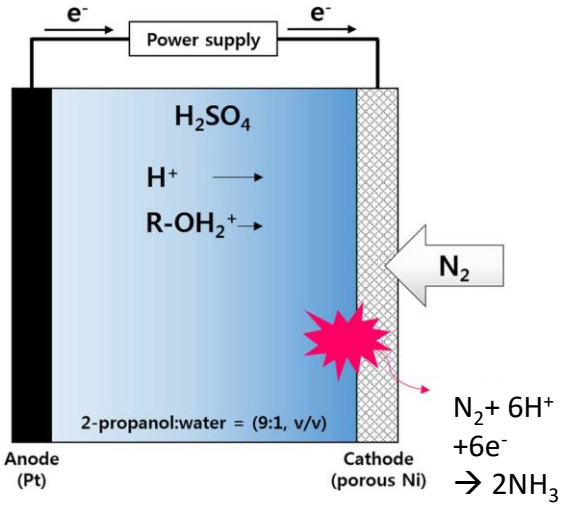

J. Electrochem. Soc. **2016**, 163 (7) F610

- Porous Ni
- IPA:Water (9:1 v/v) 10mM H_2SO_4 (IPA: isopropyl alcohol)
- Ammonia production rate (r_{NH3-N}): 1.54×10^{-11} mol s^{-1} cm^{-2}
- Faradic efficiency (FE): 0.8 %

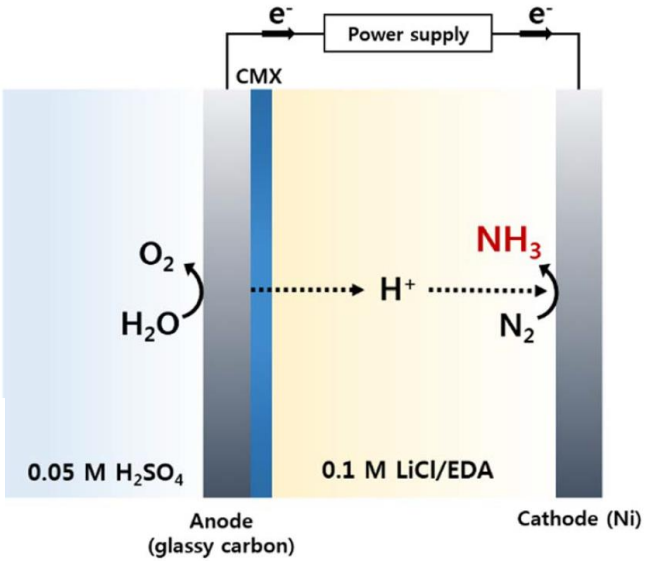

J. Electrochem. Soc. **2016**, 163 (14) F1523

- Porous Ni
- Anodic compartment : 0.05 M H_2SO_4
- Cathodic compartment: 0.1 M LiCl/Ethylenediamine (EDA)
- r_{NH3-N}: 3.58×10^{-11} mol s^{-1} cm^{-2}
- FE: 17.2 %

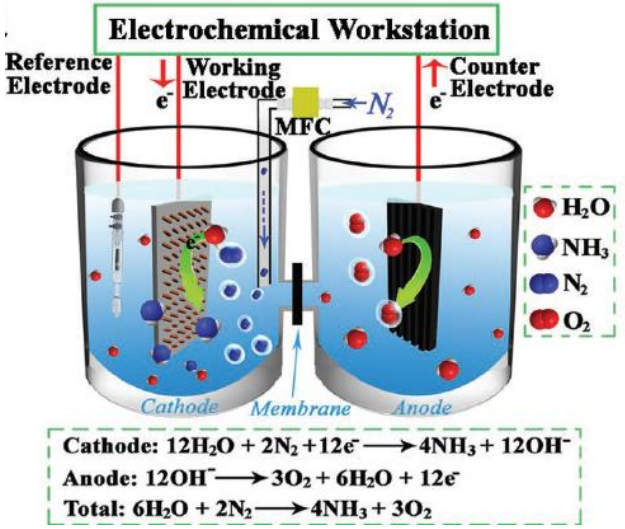

Adv. Mater. **2017**, 29 (3), 1604799

- Tetrahexahedral Au nanorods
- 0.1 M KOH, 2 compartment cell
- r_{NH3-N}: 1.648 μg h^{-1} cm^{-2}
- FE: 4.0 %

Possible Strategies to Improve Selectivity

- **Limit the proton transfer rate by**

  Reducing the conc. of protons in the bulk solution

  Increasing the barrier for proton transfer to the surface

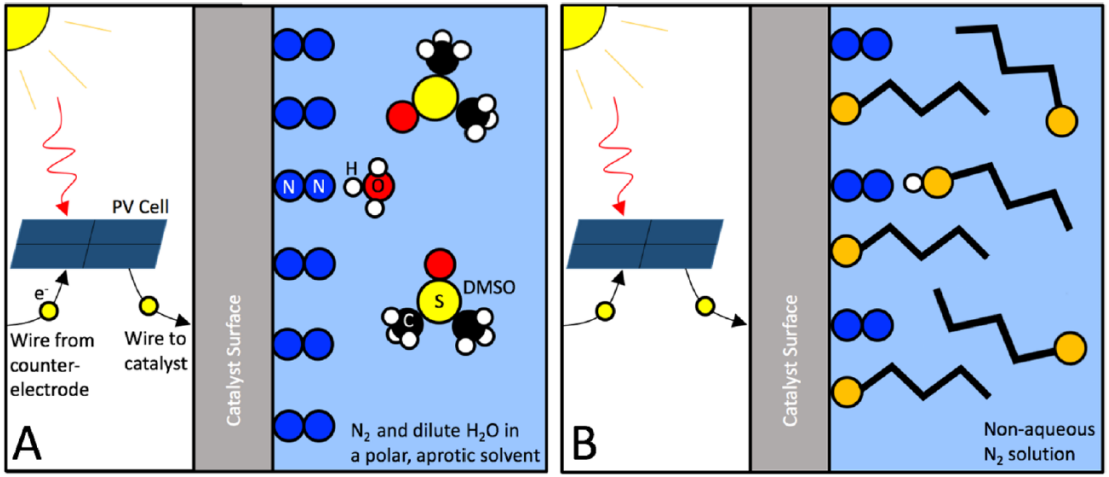

- **Limit the electron transfer rate by**

  requiring electrons to tunnel through a thin insulator,

  using photoabsorbers to supply a slow s tream of electrons

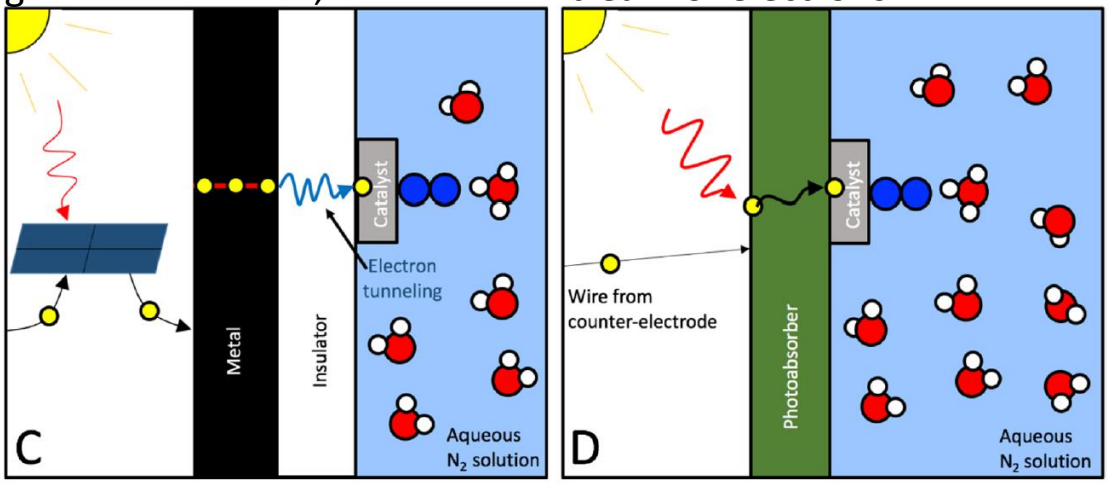

5

A. Singh et al., ACS Catalysis, 2017, 7, 706

Generic Mechanisms for N_2 Reduction to NH_3

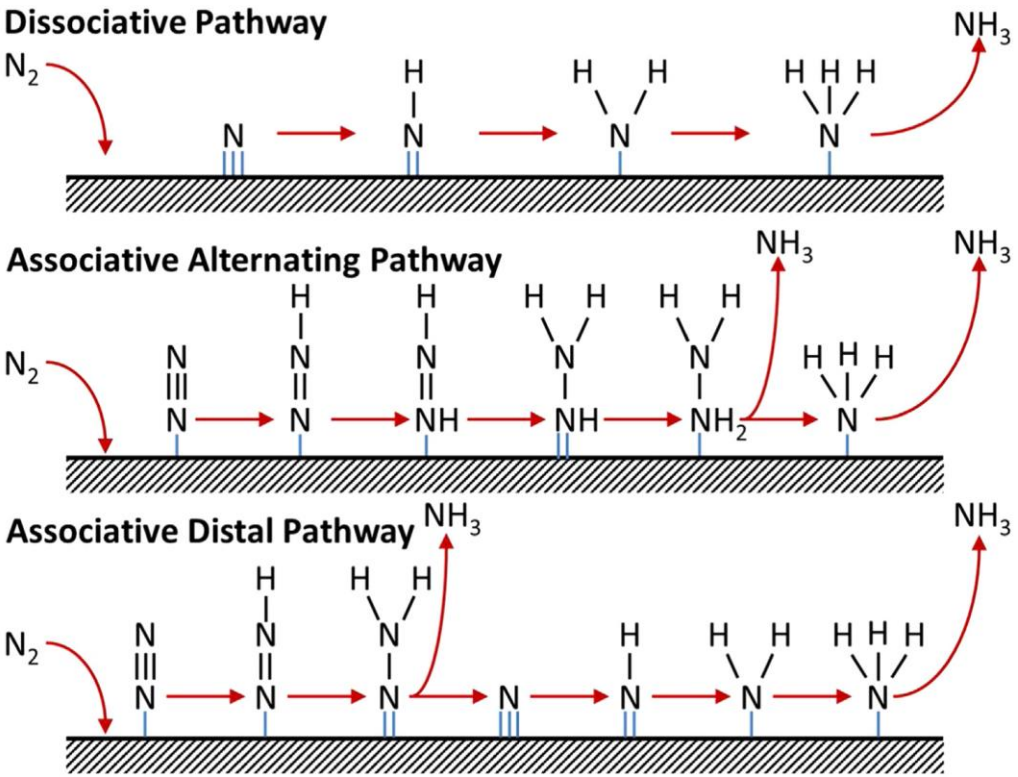

Catal. Today 2016

- Dissociative mechanism : NΞN bond is broken before any hydrogenation take place.
  → Haber Bosch process operates through a dissociative mechanism.
- Associative alternating pathway : Hydrogenation events in each of the two nitrogen centres
  → One nitrogen is converted into NH_3 and the NΞN bond is broken.
- Associative distal pathway : Hydrogenation occurs on the furthest away from the surface
  → The release of one equivalent of NH_3 → metal nitrido (MΞN) unit will be hydrogenated to give 2nd NH_3

Volcano Plot for Ammonia Production by DFT

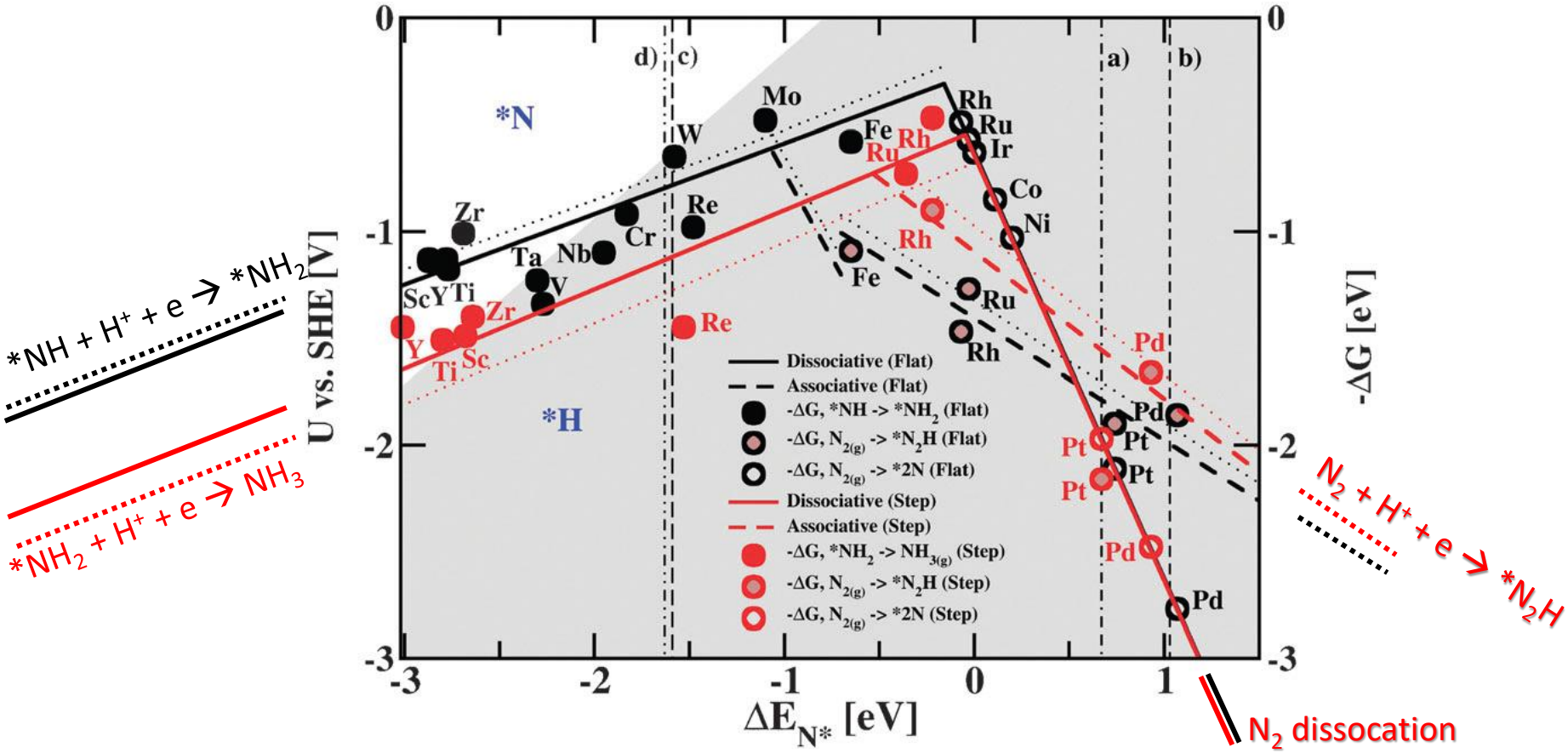

Phys. Chem. Chem. Phys., 2012, **14**, 1235–1245

- The most active surfaces are Mo, Fe, Rh, and Ru, but hydrogen gas formation will be a competing reaction reducing the faradaic efficiency for ammonia production.
- Sc, Y, Ti, and Zr bind N-adatoms more strongly than H-adatoms.

Ammonia Production by Metal Nitride

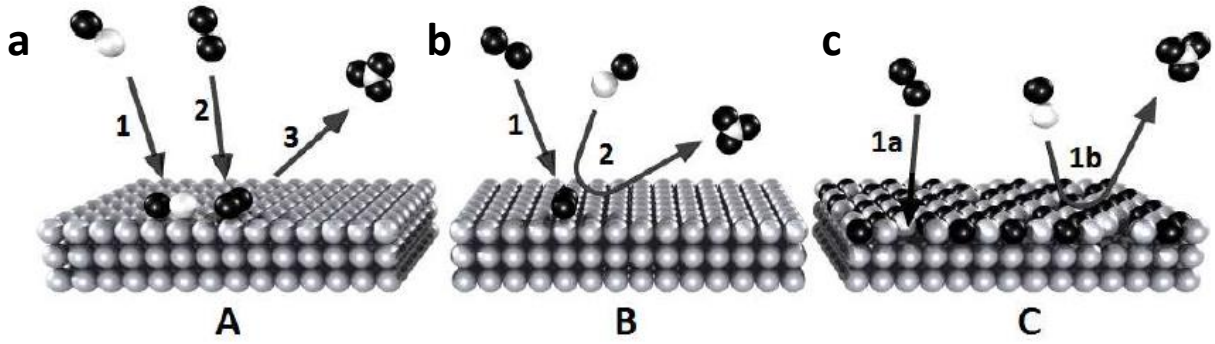

(a)Langmuir-Hinshelwood mechanism
Both reactants first adsorb onto the surface (reaction 1 and 2), before a reaction takes place.

(B) Eley-Rideal mechanism
Only one of the reactants adsorbs onto the surface (reaction 1).

(c) Mars-van Krevelen mechanism
The surface itself is an active part in the reaction: one reactant forms a chemical bond with the catalytic surface (reaction 1a), forming a thin surface layer of Metal-Reactant.

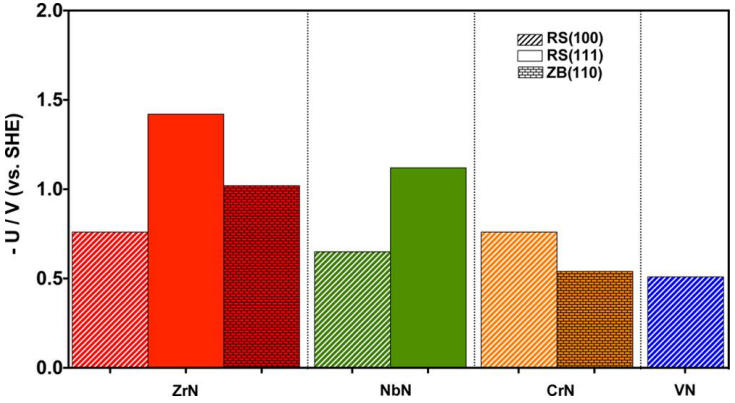

*ACS Catal. 2016, **6**, 635−646*

- Metal nitrides can further enhance the catalytic property by way of a Mars-van Krevelen mechanism.
- The vacancy is likely refilled by N and thus the catalytic cycle may continue to form the second NH_3.

Efficient Photocatalytic Nitrogen Fixation: Enhanced Polarization, Activation, and Cleavage by Asymmetrical Electron Donation to N≡N Bond

Jili Yuan, Xuanying Yi, Yanhong Tang, Meijun Liu, and Chengbin Liu**

Adv. Funct. Mater. **2019**, 1906983 https://doi.org/10.1002/adfm.201906983

Polarization by Asymmetrical Electron Donation

Enhanced Polarization, Activation, and Cleavage

Photocatalytic nitrogen (N_2) fixation suffers from low efficiency due to the difficult activation of the strongly nonpolar N≡N bond. In this study, a Ru–Co bimetal center is constructed at the interface of Ru/CoS_x with S-vacancy on graphitic carbon nitride nanosheets (Ru-Vs-CoS/CN). Upon adsorption, the two N atoms in N_2 are bridged to the Ru–Co center, and the asymmetrical electron donation from Ru and Co atoms to N_2 adsorbate highly polarized N≡N bond to double bond order. The plasmonic electric-field-enhancement effect enables the Ru/CoS_x interface to boost the generation of energetic electrons. The Schottky barrier between Ru and CoS_x endows the interface with electron transfer from CoS_x to Ru. The Ru-end bound N at the Ru–Co center is preferentially hydrogenated. As a result, the Ru-Vs-CoS/CN photocatalyst shows an NH_3 production rate of up to 0.438 mmol g^{-1} h^{-1}, reaching a high apparent quantum efficiency of 1.28% at 400 nm and solar-to-ammonia efficiency of 0.042% in pure water under AM1.5G light irradiation.

- Nonpolar N2 molecules are adsorbed to the Ro-Co center of the Ro-CoS catalyst.
- N2 is polarized by electrons asymmetrically supplied at the center of Ru-Co.
- Ru-CoSx with S-vacancy catalysts form a Schottky barrier between Ru-Co and the plasmonic effect resulting from the nanoscale.
- Therefore, N bonded to Ru- first undergoes hydrogenation.

Adv. Funct. Mater. **2019**, 1906983 https://doi.org/10.1002/adfm.201906983

Polarization by Asymmetrical Electron Donation

Proposed pathway on Ru-Vs-CoS/CN

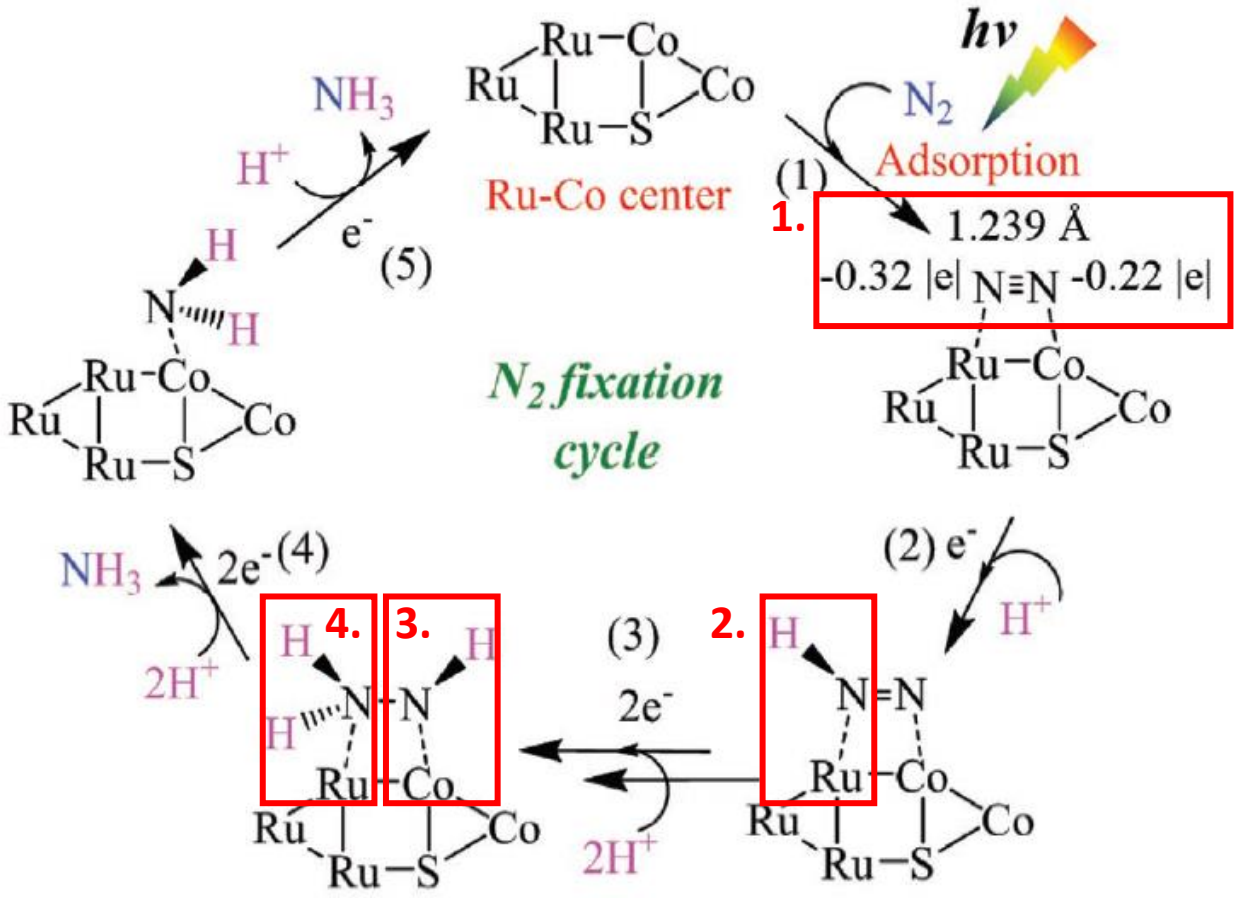

Scheme 1. Proposed photocatalytic N_2RR pathway on Ru-Vs-CoS/CN.

- Nonpolar N2 molecules are adsorbed to the Ro-Co bimetal center of the Ro-CoS with S-vacancy catalyst.
- Asymmetrical electron donation from Ru-Co atoms serves to N2 adsorbate highly polarized triple N bond.
- Plasmonic metals(Ru- nanoparticle) donate energetic electrons to N2 adsorbates.
- Plasmonic Ru/CoS interface enhances light absorption to produce energetic charge-carriers, accelerates charge separation and transfer, and thus kineticaaly facilitates N2 fixation.

Adv. Funct. Mater. **2019**, 1906983 https://doi.org/10.1002/adfm.201906983

Polarization by Asymmetrical Electron Donation

DFT calculations

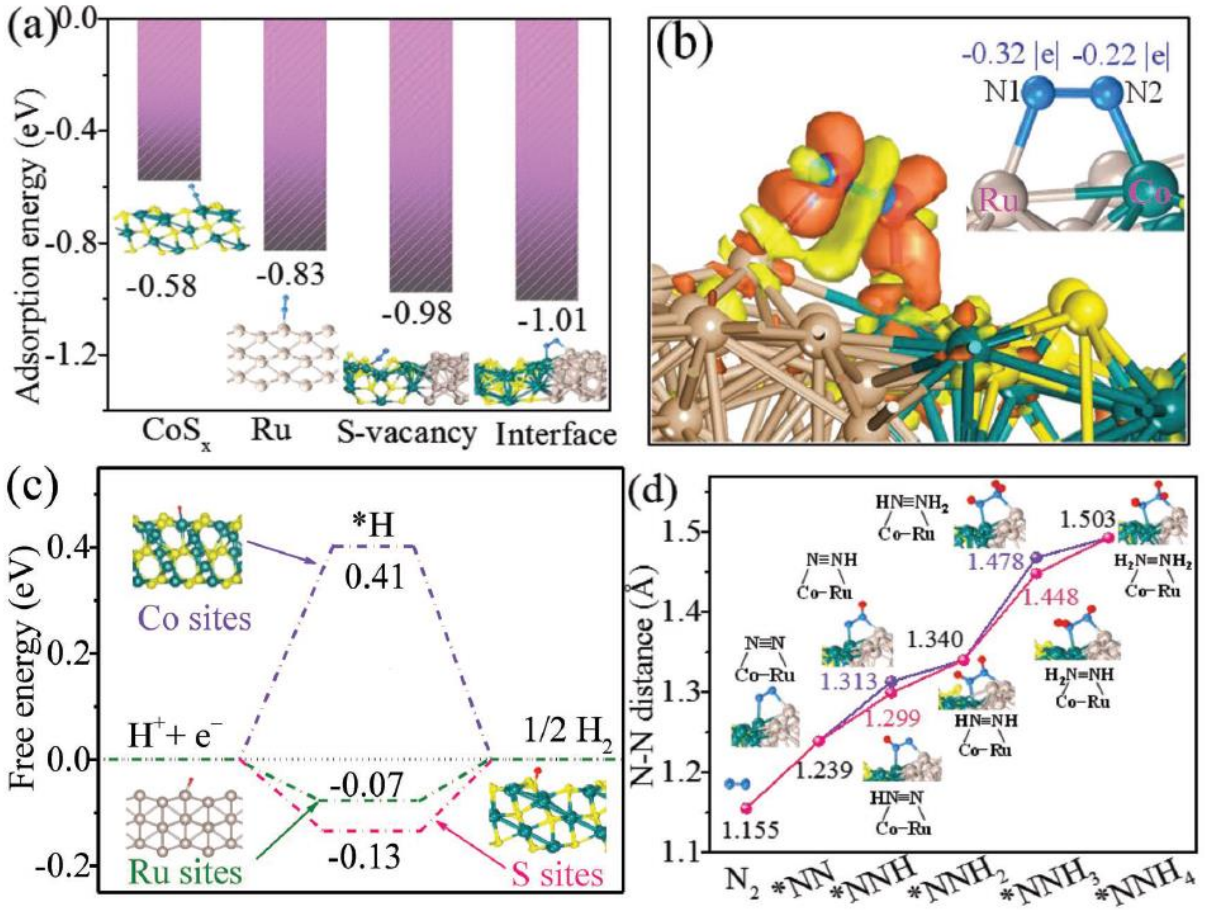

- **(a)** shows adsorption energies of N2 on single sith of Ru, Co (or S-vacancy) in CoSx, and on Ru-Co center at Ru/CoSx interface.
- **(b)** show differential charge density of Ru/CoSx interface
- **(c)** show free energy of HERs on Ru and Co (or S) in CoSx. The HER was limited by *H adsorption on the Co of CoSx and by *H desorption on the S of CoSx
- **(d)** show N–N distances of free N2 and intermediates during hydrogenation starting from the N on Ru or Co

Adv. Funct. Mater. **2019**, 1906983 https://doi.org/10.1002/adfm.201906983

Polarization by Asymmetrical Electron Donation

DFT calculations

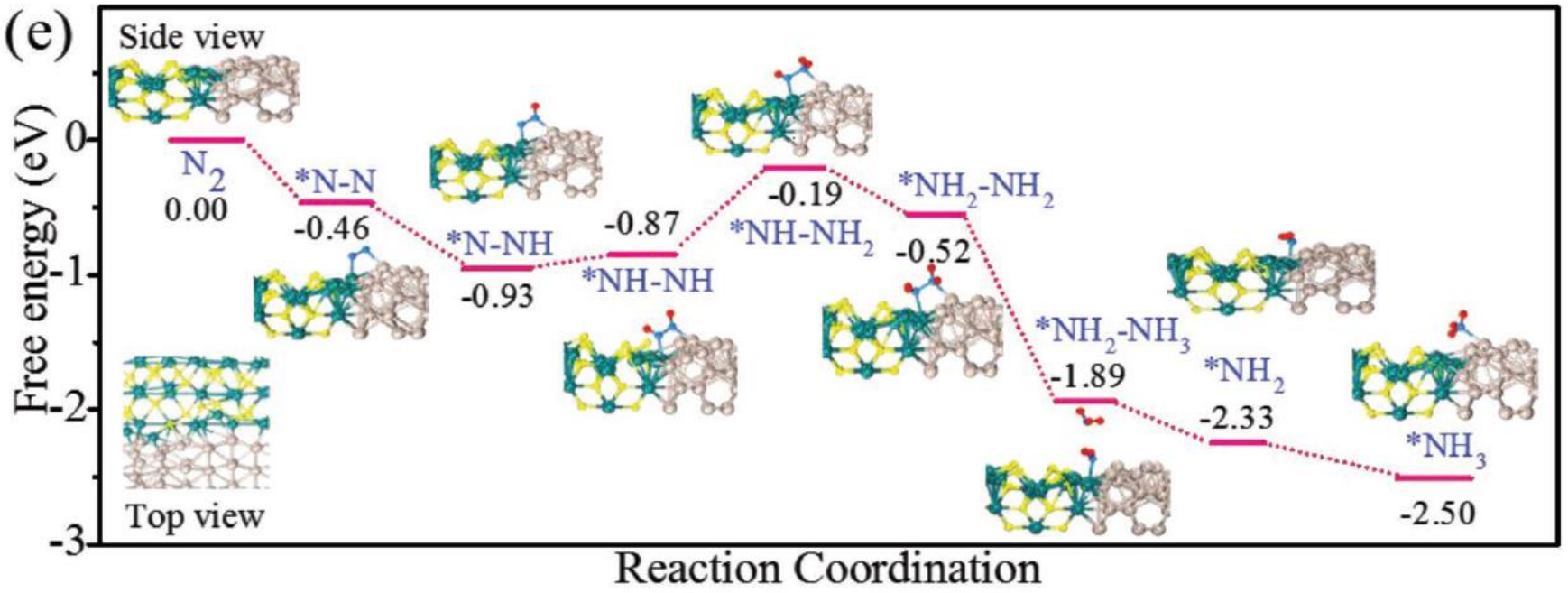

- Calculatedd N2RR pathway on Ru(001)/CoSx(101) interface.

Adv. Funct. Mater. **2019**, 1906983 https://doi.org/10.1002/adfm.201906983

Polarization by Asymmetrical Electron Donation

TEM analysis

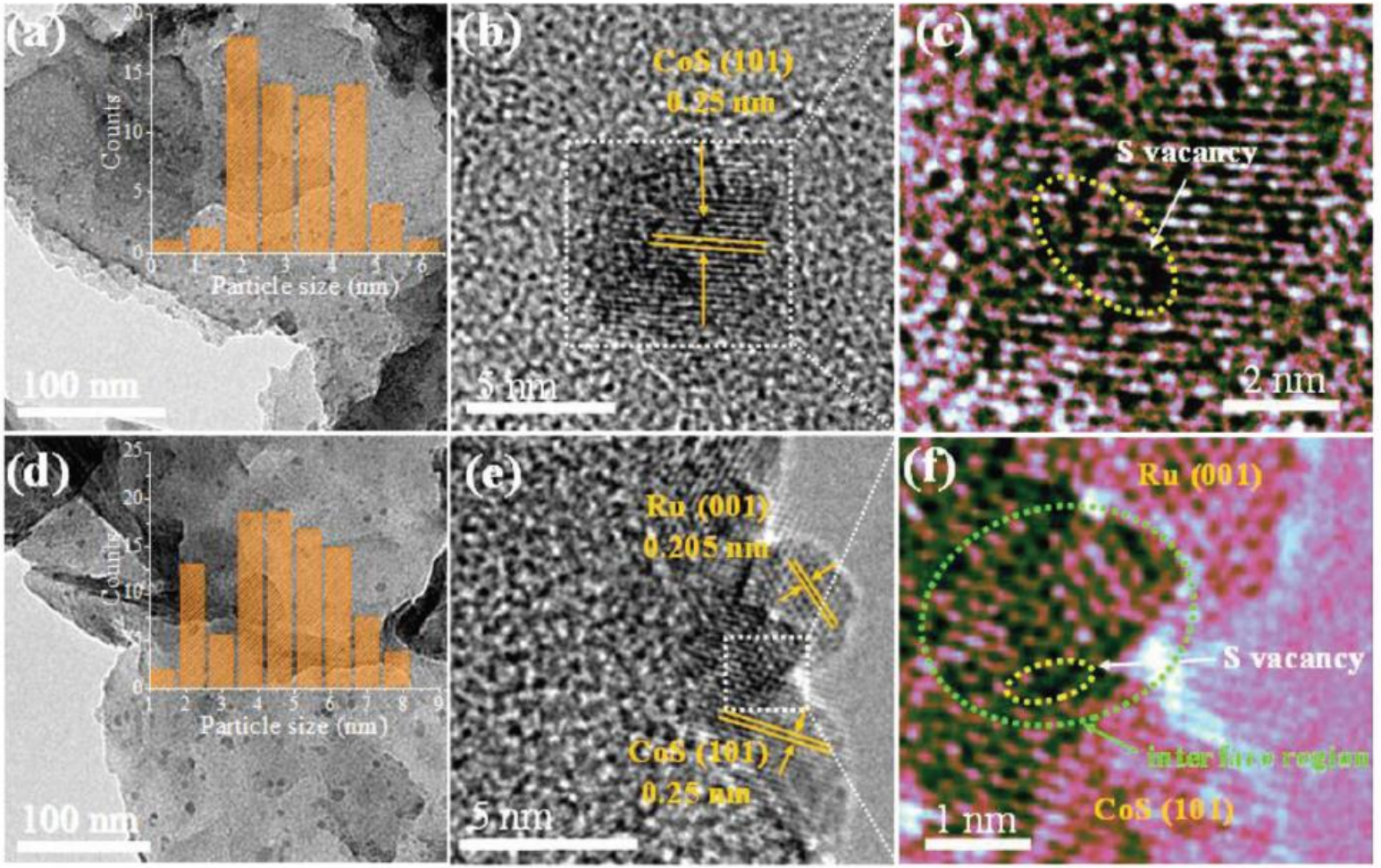

Adv. Funct. Mater. **2019**, 1906983 https://doi.org/10.1002/adfm.201906983

Polarization by Asymmetrical Electron Donation

FT-IR analysis

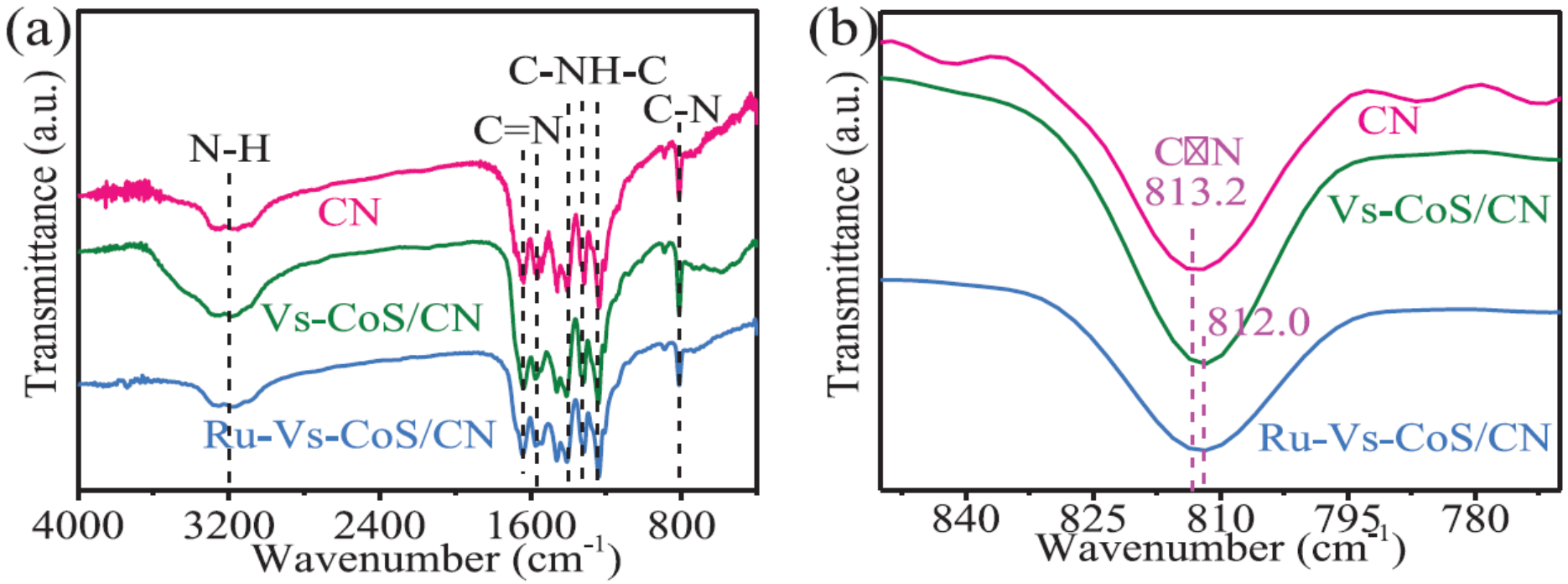

- Fourier transform infrared (FT-IR) spectra reflect the characteristic features of g-C3N4.
- The C–N peak slightly shifts from 813.2 cm^{-1} for CN to 812 cm^{-1} for Vs-CoS/CN and Ru-Vs-CoS/CN.
- It indicate a decreasing electron cloud density of N due to the coordination of lone pair electrons of sp3-N with the unoccupied d orbitals of Co or Ru.

Adv. Funct. Mater. **2019**, 1906983 https://doi.org/10.1002/adfm.201906983

Polarization by Asymmetrical Electron Donation

UV-vis-NIR absorption and FDTD-simulation

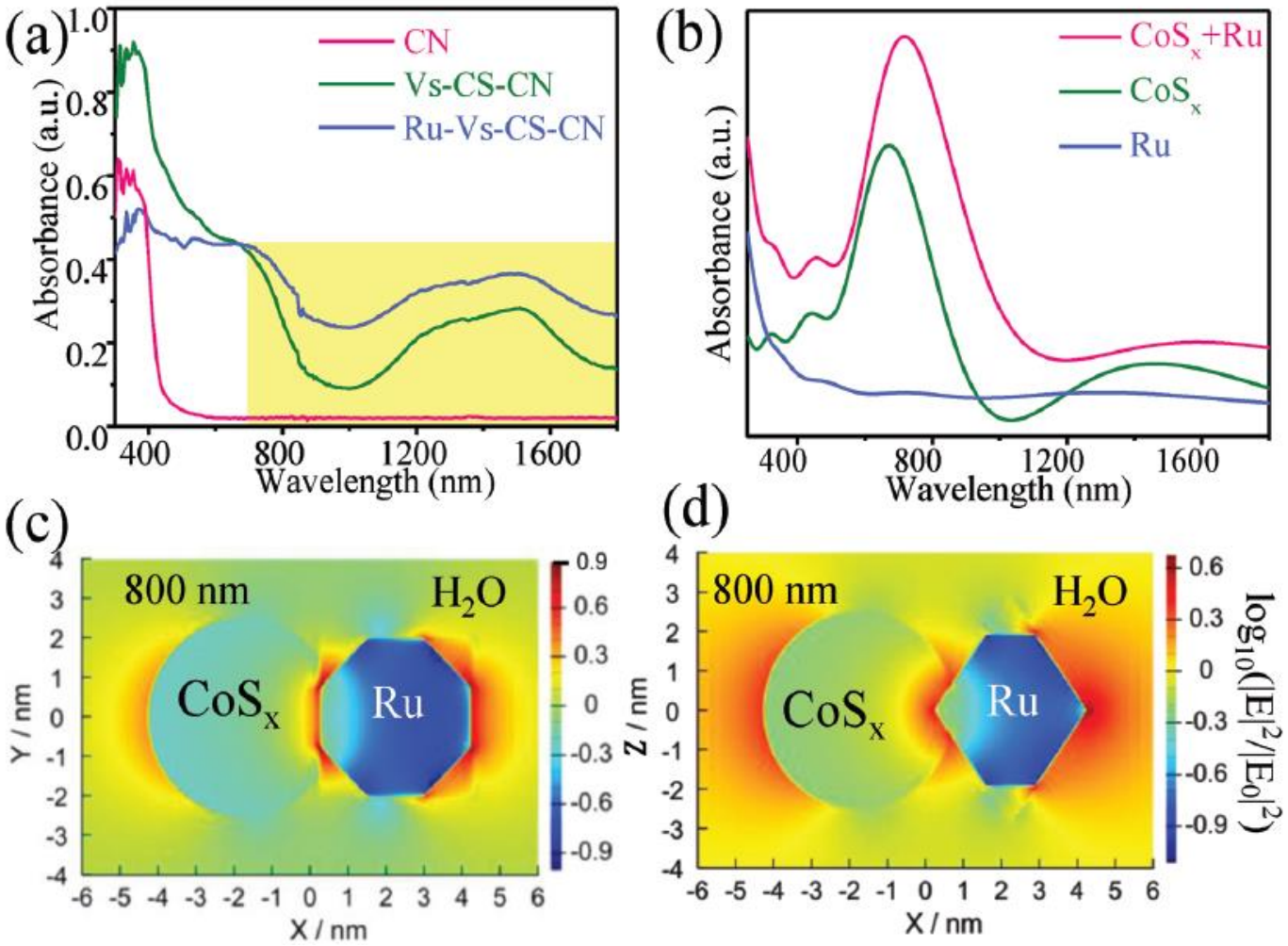

Adv. Funct. Mater. **2019**, 1906983 https://doi.org/10.1002/adfm.201906983

Polarization by Asymmetrical Electron Donation

Photocatalytic results

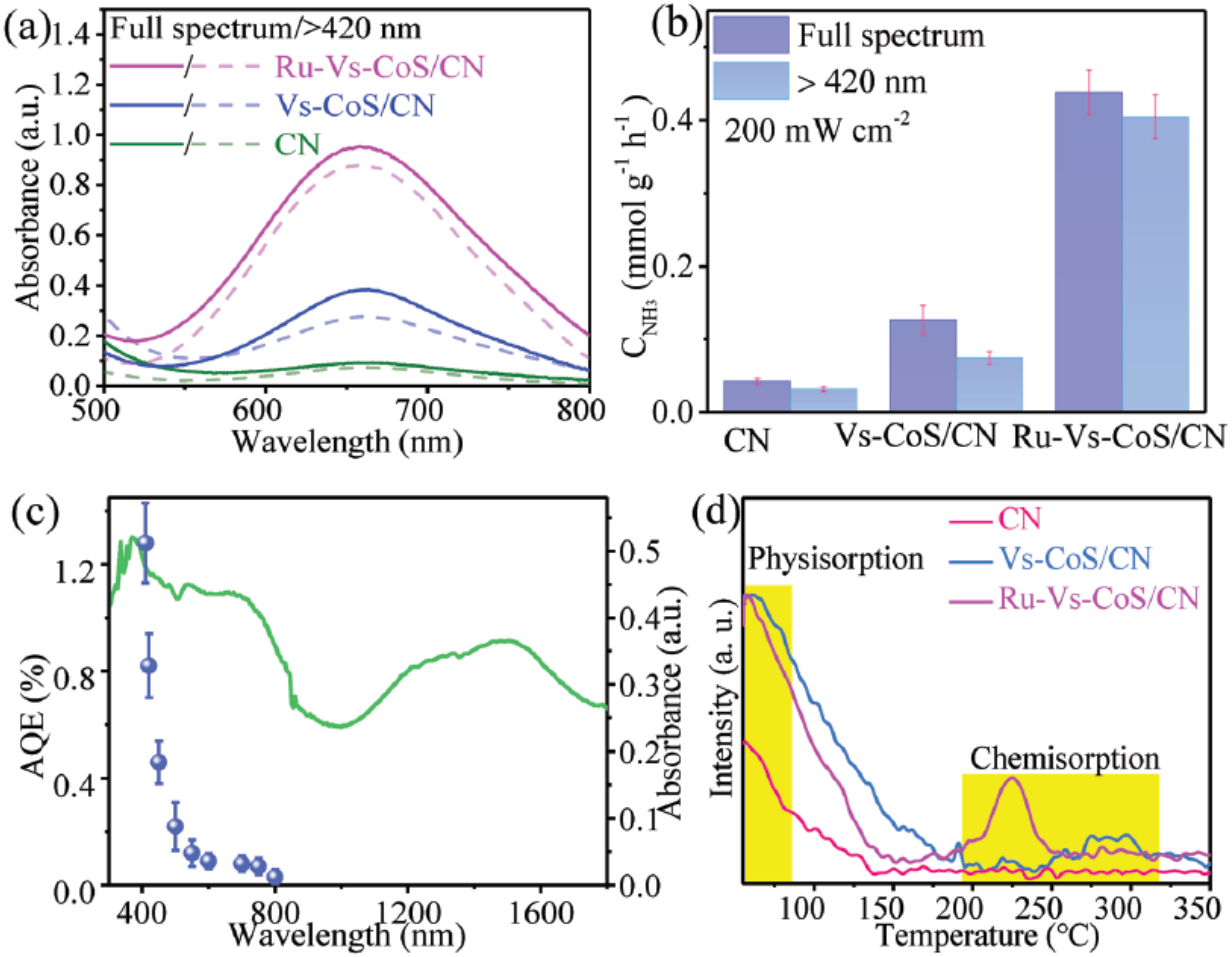

Figure 4. Photocatalytic N_2 fixation: a) UV–vis absorption spectra of reaction solution in the first 1 h (solid lines for full spectrum; dash lines for light >420 nm) and b) NH_3 production rates. Conditions: 200 mW cm^{-2}, methanol sacrificial agent. c) AQEs (blue dots) for N_2 fixation over Ru-Vs-CoS/CN in pure water under monochromatic light irradiation in reference to its UV–vis spectra (green line). d) N_2-TPD profiles of the photocatalysts.

Adv. Funct. Mater. **2019**, 1906983 https://doi.org/10.1002/adfm.201906983

Theoretical Strategies to Overcome ENRR

Operando Oxygen Vacancies for Enhanced Activity and Stability toward Nitrogen Photofixation

Tingting Hou, Yu Xiao, Peixin Cui, Yining Huang, Xiaoping Tan, Xusheng Zheng, Ying Zou, Changxi Liu, Wenkun Zhu, Shuquan Liang,* and Liangbing Wang**

Photocatalysts with oxygen vacancies (OVs) have exhibited exciting activity in N_2 photofixation due to their superiority in capture and activation of N_2. However, the surface OVs are easily oxidized by seizing the oxygen atoms from water or oxygen during the catalytic reaction. Here, it is reported that the grain boundaries (GBs) in nanoporous WO_3 induce plenty of operando OVs under light irradiation to significantly boost catalytic activity toward N_2 photofixation. Impressively, nanoporous WO_3 with abundant GBs (WO_3-600) exhibit an ammonia production rate of 230 μmol $g_{cat.}^{-1}$ h^{-1} without any sacrificial agents at room temperature, 17 times higher than that for WO_3 nanoparticles without GBs. Moreover, WO_3-600 also manifests remarkable stability by maintaining nearly ≈100% catalytic activity after ten successive reaction rounds. Further mechanistic studies reveal that both OVs and GBs regulate the band structures of WO_3 nanocrystals, as well as favor the delivery of photogenerated electrons to adsorbed N_2 by enhancing W–O covalency. More importantly, plenty of operando OVs induced by GBs generate during catalytic reaction, directly contributing to the excellent catalytic performance for WO_3-600. This work opens a novel avenue to developing efficient photocatalysts by construction of operando OVs.

Adv. Energy Mater. **2019**, *9*, 1902319
https://doi.org/10.1002/aenm.201902319

Theoretical Strategies to Overcome ENRR

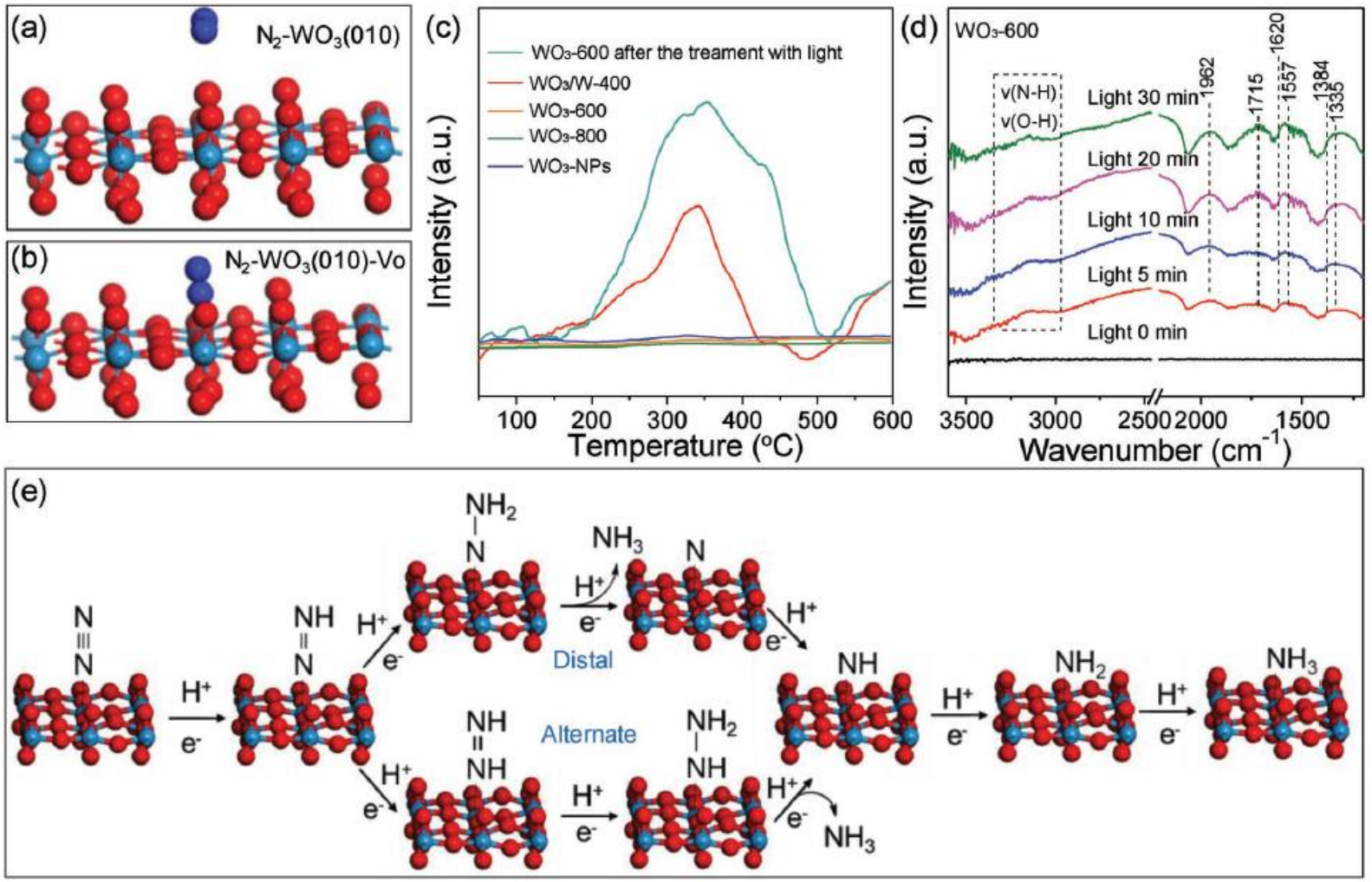

Figure 5. The adsorption configuration of N_2 molecule on the surface of a) WO_3(010) and b) WO_3(010)-Vo. c) N_2-TPD profiles of WO_3/W-400, WO_3-600, WO_3-800, WO_3-NPs, and WO_3-600 after the treatment with light. d) In situ DRIFT spectra recorded during the photocatalytic N_2 fixation over WO_3-600. e) The possible reaction pathways for N_2 photofixation over WO_3-600. The red, light blue and dark blue balls represent O, W, and N atoms, respectively.

Support info. - Detail figure

Operando Oxygen Vacancies for Enhanced Activity and Stability toward Nitrogen Photofixation

Tingting Hou, Yu Xiao, Peixin Cui, Yining Huang, Xiaoping Tan, Xusheng Zheng, Ying Zou, Changxi Liu, Wenkun Zhu, Shuquan Liang,* and Liangbing Wang**

Support info. - Detail figure

Operando Oxygen Vacancies for Enhanced Activity and Stability toward Nitrogen Photofixation

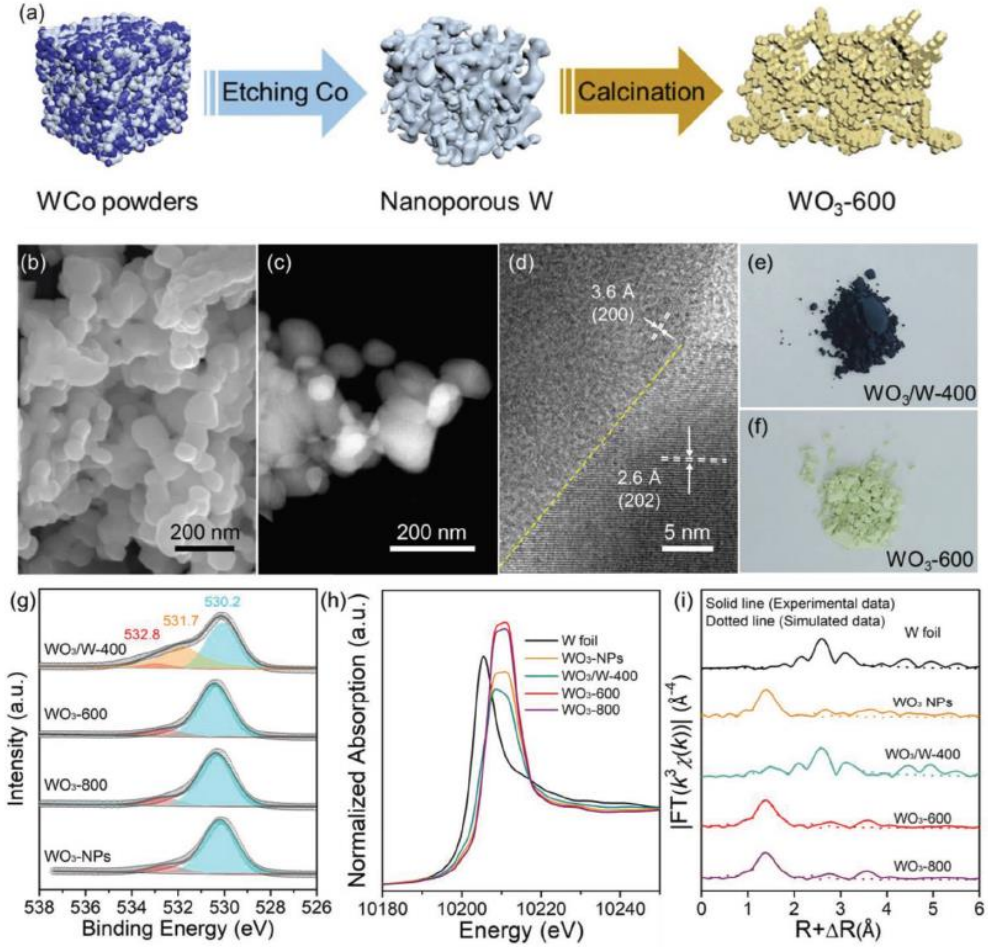

Figure 1. a) Schematic diagram for the synthetic process of the photocatalysts. b) SEM image, c) HAADF-STEM image, and d) HRTEM image of WO_3-600. The pictures of e) WO_3/W-400 and f) WO_3-600. g) O 1s XPS spectra, h) XANES spectra, and i) Fourier-transformed EXAFS spectra in R space for WO_3/W-400, WO_3-600, WO_3-800, and WO_3-NPs (W foil was used as the reference).

Support info. - Detail figure

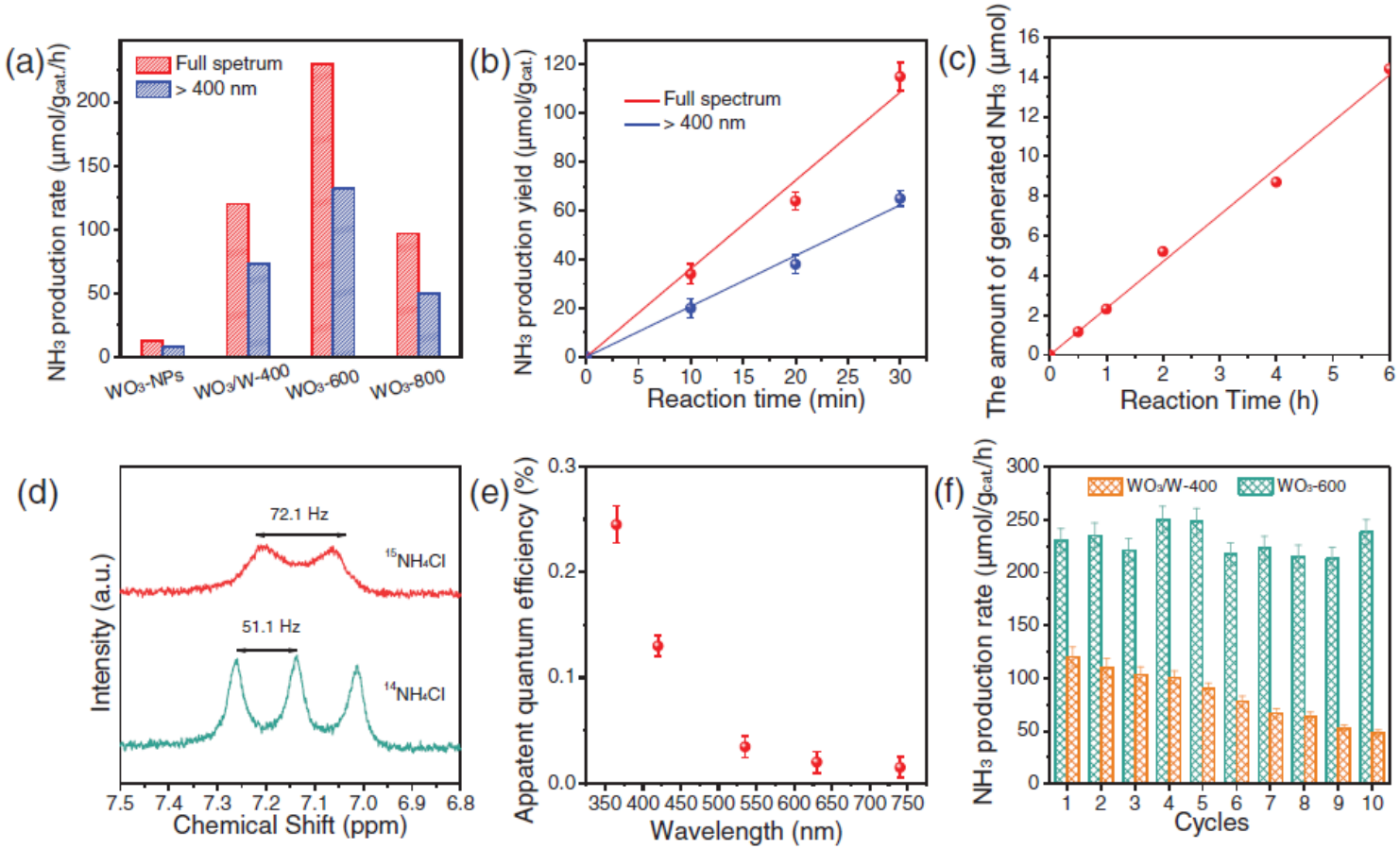

Figure 2. a) Photocatalytic NH_3 production rates over WO_3-NPs, WO_3/W-400, WO_3-600, and WO_3-800. b) Time courses of the N_2 fixation over WO_3-600 under irradiation of full spectrum and visible light (>400 nm). c) The amount of generated NH_3 with the reaction time catalyzed by 10 mg of WO_3-600. d) ^{1}H-NMR (400 MHz) spectra of solution after photocatalytic N_2 fixation by using WO_3-600 as the photocatalyst in $^{14}N_2$ or $^{15}N_2$ atmosphere. e) Calculated AQEs for N_2 fixation over WO_3-600 under monochromatic light irradiation. f) NH_3 production rates for WO_3-600 and WO_3/W-400 over the course of ten rounds of successive reaction.

Support info. - Detail figure

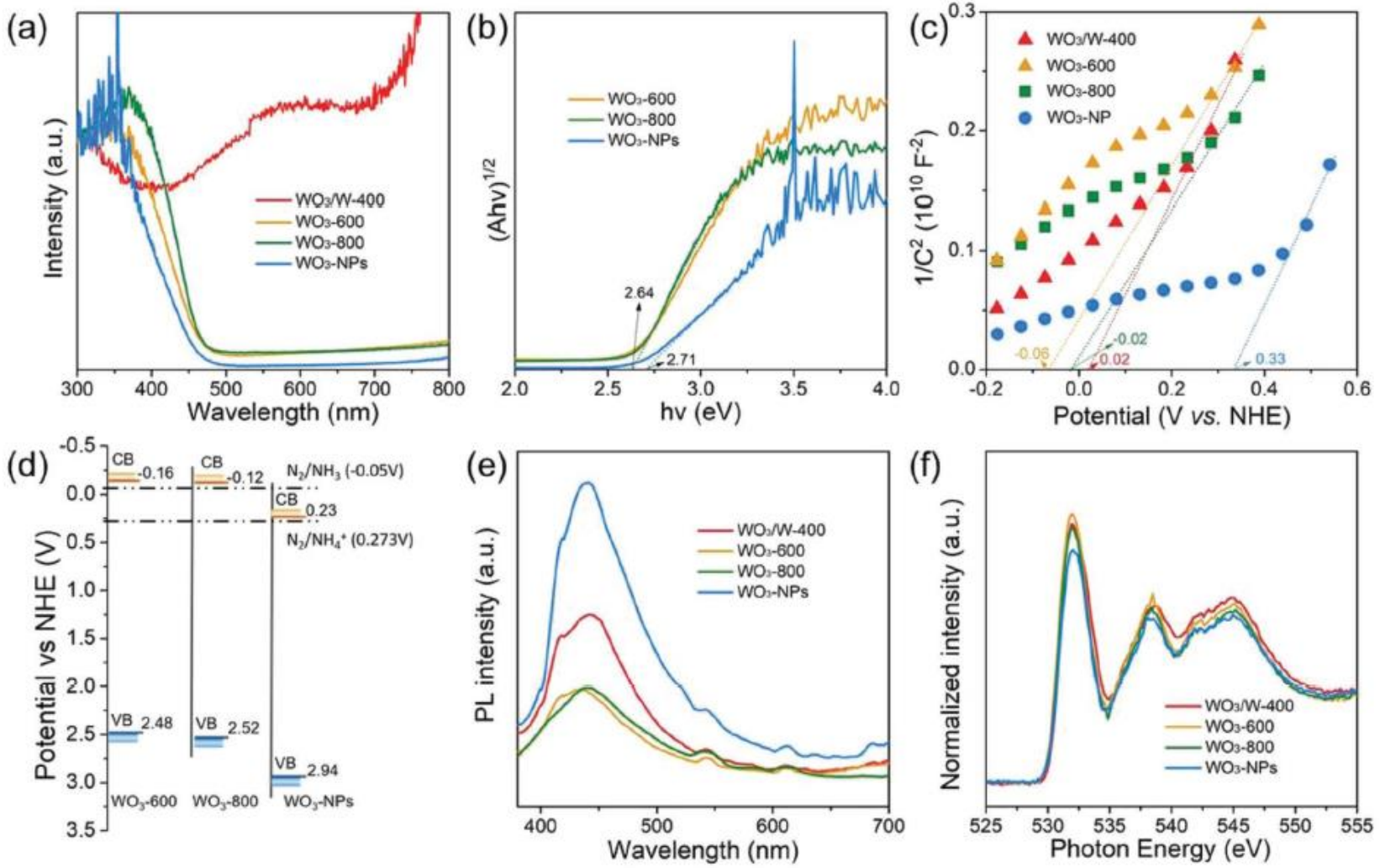

Figure 3. a) Diffuse reflectance UV–vis spectra, b) transformed Kubelka-Munk function and c) Mott-Schottky plots of the as-prepared photocatalysts. d) The illustration of band structures of WO_3-600, WO_3-800, and WO_3-NPs. e) Room-temperature steady-state PL spectra and f) O K-edge XAS spectra of the as-prepared photocatalysts.

Support info. - Detail figure

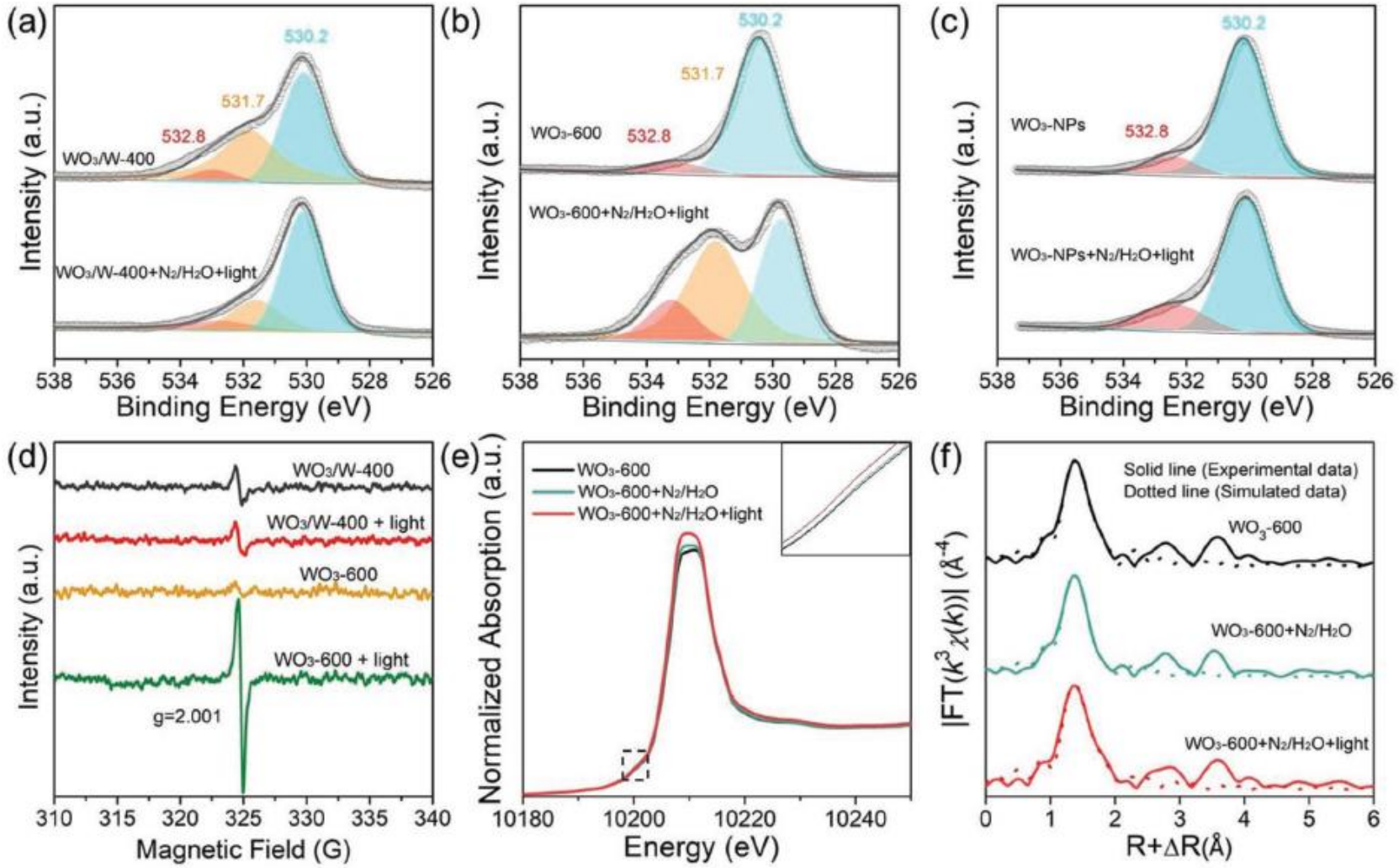

Figure 4. Quasi in situ XPS spectra of O 1s in a) WO_3/W-400, b) WO_3-600, and c) WO_3-NPs before and after treatment. d) In situ ESR spectra of WO_3/W-400 and WO_3-600 before and after light irradiation. In situ e) XANES and f) Fourier-transformed EXAFS spectra in R space of WO_3-600.

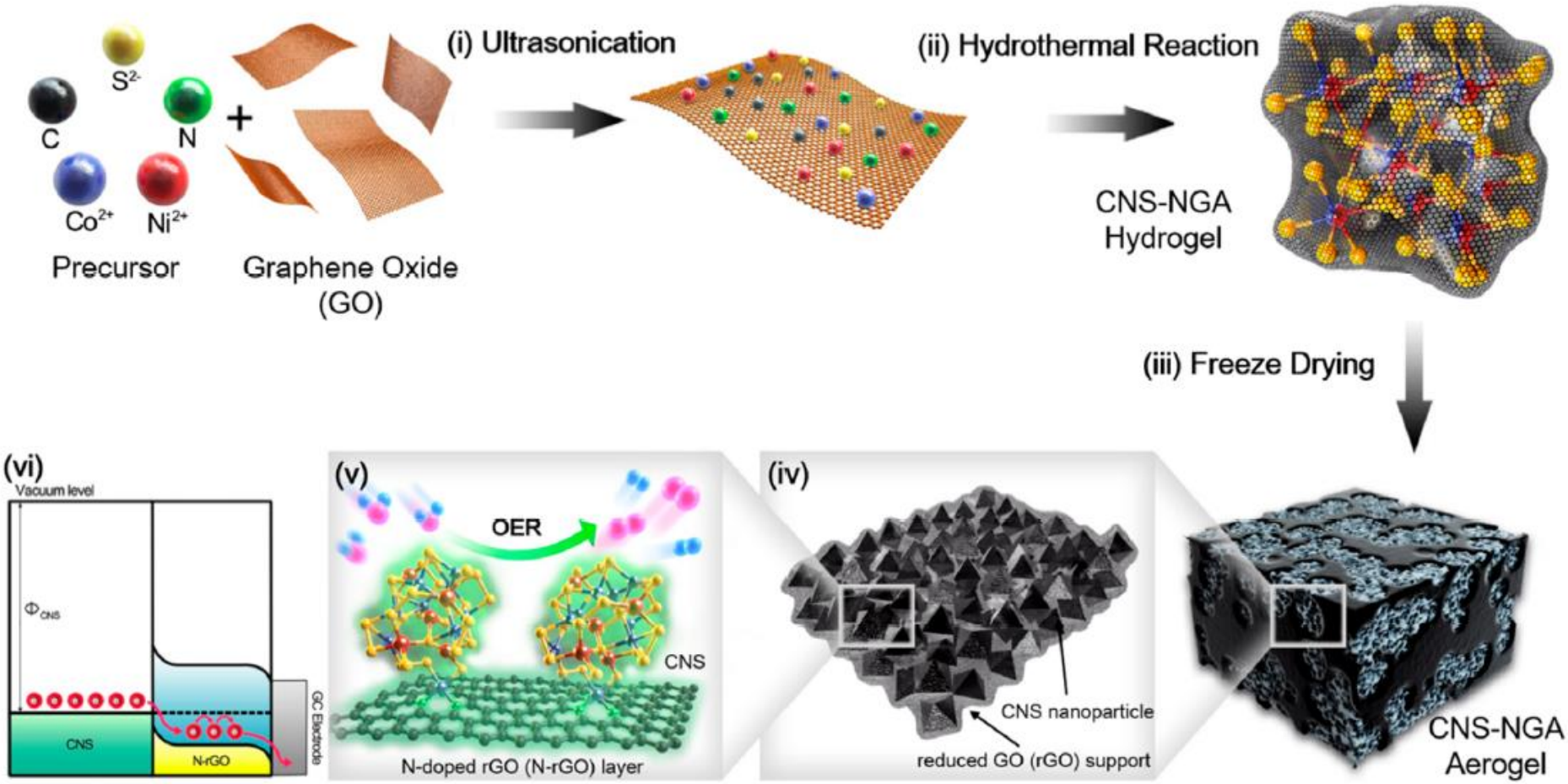
S2-
C
N
Co2+
Ni2+
Precursor
+
Graphene Oxide
(GO)
(i) Ultrasonication
(ii) Hydrothermal Reaction
CNS-NGA
Hydrogel
(iii) Freeze Drying
(vi)
Vacuum level
ΦCNS
CNS
N-rGO
GC Electrode
(v)
OER
CNS
N-doped rGO (N-rGO) layer
(iv)
CNS nanoparticle
reduced GO (rGO) support
CNS-NGA
Aerogel